NISS

Influence of Microstructure and Fracture on the Transport Properties in Cement-Based Materials

Sanjay S. Jaiswal, Takeru Igusa, Trish Styer,
Alan F. Karr and Surendra P. Shah

Technical Report Number 61
July, 1997

National Institute of Statistical Sciences
19 T. W. Alexander Drive
PO Box 14006
Research Triangle Park, NC 27709-4006
www.niss.org

INFLUENCE OF MICROSTRUCTURE AND FRACTURE ON THE TRANSPORT PROPERTIES IN CEMENT-BASED MATERIALS

Sanjay S. JAISWAL[1], Takeru IGUSA[1], Trish STYER[2], Alan KARR[2] and Surendra P. SHAH[1]

[1]NSF Center for Advanced Cement-Based Materials
2145 Sheridan Road, A130
Evanston, IL - 60208, USA

[2]National Institute of Statistical Sciences
PO Box 14162, Research Triangle Park,
North Carolina 27709-4162, USA

ABSTRACT

Durability of concrete structures requires an integrated approach consisting of permeability, cracking resistance, and strength of material. Permeability is influenced by the volume fraction of the aggregate, the interfacial zone around each aggregate, many factors related to material heterogeneities including tortuosity of ion path around the aggregates, and cracking. A systematic study is being conducted at NSF Center for ACBM at Northwestern University to study the effect of above parameters on chloride and water permeability of concrete. Initial results indicate that a simple definition of tortuosity and interfacial zone around each aggregate can be used to interpret rapid chloride permeability (ASTM C1202-93) results for a composite consisting of alumina spheres and cement matrix. Preliminary models using conductivity and percolation concepts are used to further explain the conclusions. The influence of cracks on permeability in paste, normal strength concrete (NSC) and high strength concrete (HSC) is examined using a feedback controlled splitting tensile test. Effect of crack roughness on water permeability measurements has been quantified using laminar flow through a parallel sided slot with modifications for crack geometry. Water and rapid chloride permeability of NSC and HSC slices is also described and compared.

INTRODUCTION

For several decades, concrete quality has been specified by its compressive strength. Recently, there has been a shift from strength to an integrated approach involving strength, permeability and cracking [1]. Permeability controls the migration of fluids, both liquids and gases, through the microstructure and mesostructure of concrete. Microstructure of concrete, at the scale 10^{-6} m, is characterized by grains, surfaces, interfaces and defects, involving phase fractions, orientations, sizes, shapes, the spatial distribution of phase domains and connectivity of phases [2]. Permeable microstructure includes gel and capillary pores in cement paste, voids in the weak matrix-aggregate interfacial zone and microcracks due to volumetric changes. Mesostructure of concrete ($\sim 10^{-3}$m), which includes aggregates, air voids, and macrocracks, also influences permeability by providing obstacles to the macro flow of liquids and gases. Hence, permeability in concrete is characterized by wide range of feature sizes, from nanometer pores to centimeter size aggregates. For any study of permeability of concrete to be valid, permeability of samples should be large compared to the length scale (correlation length) of the heterogeneities so that average flow rates can be used to analyze the system [3].

The flow in porous media, such as concrete, has traditionally been described using continuum and discrete models. Continuum modeling is the classical engineering approach for describing complex materials like concrete, characterized by several length scales. Effective properties of a porous medium are defined as the averages of corresponding microscopic quantities. The averages must be taken over a volume small enough compared to the volume of the system, but large enough for applicable equations of change (Darcy's law, Fick's Law etc.) to hold when applied to that volume [3]. Predictions are difficult due to complex nature of the system (length scales and interconnectivity) and many empirical factors are often added to account for disparities between theoretical and experimental results. Discrete models on the other hand do not suffer from these limitations because the description can be anywhere from sub-microscopic level to megascopic levels. These models are based on a discretized description of the material in terms of networks. The only difficulty is the amount of computational effort required and knowledge of applicable mathematical equations. Some of the ideas applied included percolation theory, diffusion processes, fractal concepts and universal scaling laws, which describe how and under what conditions the effective macroscopic properties of the system may be independent of its microscopic details [3].

Recent research has shown that permeability of concrete is influenced by volume fraction of the aggregate, the tortuosity of the path of the ions or water molecules around the aggregate, and the interfacial zone around each of these aggregates. Introduction of aggregates reduces the area for the permeation of the ions in the concrete microstructure because the aggregates in general are less permeable than paste samples [4,5]. Aggregates have generally been modeled as non-permeable inclusions for simplicity [4,6]. This dilution or degree of reduction of permeability of paste matrix depends on amount of aggregate. A related effect is the tortuous nature of the path of the ions around the aggregates. The concept of tortuosity has been used in the literature in catalysis, biology,

porous media including concrete, and colloidal dispersions [5,7,8,9,10]. Tortuosity is traditionally used as an adjustable parameter in classical models. Increasing tortuosity leads to decreased permeability. Also, due to the so-called wall effect, there is an area of variable width around the aggregates with rarified packing as compared to the matrix. The amount of this surface area or the so-called interfacial transition zone (ITZ) increases with the amount of the aggregates present in the concrete [11,12,13,14]. The porosity and water to cement ratio in this area is much higher than surrounding matrix leading to a greater permeability around the aggregate than the matrix [11,12,14]. Hence effective permeability measured by any of the methods is the combined effect of all the above three parameters. There is a great need to study this problem for the broad understanding of permeability of concrete. Several researchers have studied parts of the problem but not the effects as a whole [10,11,12,14,15,16,17,18].

A long term study has recently been started at NSF Center for Advanced Cement-Based Materials (ACBM) at Northwestern University in collaboration with the National Institute for Statistical Sciences (NISS) at Rayleigh, North Carolina. A statistical approach is being used which incorporates aspects of both continuum and discrete models. The central issue is to construct informative, low-dimensional characterization of the microstructure and mesostructure [2]. The objectives of this project can be summarized as follows:

1. Use the statistical theory and tools to quantify the effects of parameters which can be directly measured. These parameters include mix design variable such as volume fraction, grading, w/c ratio, maximum aggregate size, and other measurable parameters such as compressive strength and elastic modulus.
2. Identify additional parameters with strong effects on permeability like tortuosity and aggregate spacing.
3. Develop a statistically based model to predict the permeability of a given specimen based on mix design variables.
4. Develop a rational method of mix design based on permeability.

The process is illustrated in *Figure 1*. Experimental designs based on statistical methods are used to cast concrete of specified mix proportions to identify and understand variables effecting permeability of concrete, both cracked and uncracked. Samples cast are tested for water and chloride permeabilities. Tested samples are then analyzed using image analysis techniques and a 3-D mesostructure reconstruction of each sample is obtained. This reconstruction leads to identification of new variables, which explain the variability in the data. New identified variables are then used to update mix proportions. The variability in the data is of two kinds, systematic and random. System variability involves changes in mix design variables and random variation is concerned with specimen-to-specimen and trial-to-trial variation (initially assumed constant). A statistical model is being developed based on experimental and 'artificial concrete' data and will be used for making permeability predictions and recommending mix design parameters. Since, the chloride permeability is measured using rapid chloride permeability test (RCPT),

some modeling issues involving conductivity, diffusivity and percolation need to be discussed.

MODELING ISSUES: RELATION BETWEEN CONDUCTIVITY AND DIFFUSIVITY

The flux of ions, J, resulting from diffusion and from the application of an electric field (electro-migration) arise from fundamentally different mechanisms. The driving force in diffusion is proportional to the concentration gradient, while the driving force in electro-migration is proportional to the voltage gradient. Nevertheless, in both instances the ions must travel through the same medium. Using physical chemistry principles, it has been shown that the same diffusion constant applies to both diffusion and electro-migration.

The basic equations for one-dimensional flux are

$$J = -D\frac{\partial c}{\partial x} \qquad \text{(diffusion)} \qquad (1)$$

$$J = -ckD\frac{\partial V}{\partial x} \qquad \text{(electro-migration)} \qquad (2)$$

where, D is the diffusion coefficient, c is the ion concentration, V is the voltage potential, k is a constant related to temperature and the valence of the ion, and x is the one-dimensional coordinate.

While the equations appear similar, there are important differences which affect practical applications. First, for macroscopically homogeneous media such as cement paste, it is possible to impose a uniform electric field with a constant voltage gradient, $\frac{\partial V}{\partial x}$. This is because the voltage depends only on the external electrical apparatus, and is independent of the ion concentration c. Under constant voltage gradients, the flux, J, becomes independent of time. However, in diffusion a constant concentration gradient, $\frac{\partial c}{\partial x}$ cannot be imposed. The concentration is typically highest at the surface of a specimen and decreases exponentially away from the surface. With such non-constant concentration gradients, the flux becomes time-dependent and is governed by a second-order differential equation. The second major difference between the above two equations is that, with moderate voltages, the driving force in electro-migration is several orders of magnitude larger than that in diffusion. Therefore, the ion flux, J, can be measured using electro-migration in only a few seconds, whereas several months are required in diffusion experiments.

Because of the rapidity and ease of electro-migration experiments and the close relation between diffusion and electro-migration, it has become common to replace

diffusion experiments with RCPT. However, researchers working with cement and concrete have found that many other factors must be considered in the equations for ion flux. In both diffusion and electro-migration, ion-ion interaction and ionic binding of cement paste have been shown to be important factors. Furthermore, in electro-migration all ions in the paste pore solution must be included in conductivity measurements, and possible electric interactions with cement additives must be examined. These physical chemistry considerations have been published elsewhere [19,20]; in the present paper, an entirely different set of modeling issues is addressed.

While cement paste can be macroscopically modeled as a homogeneous medium, aggregate gives concrete a distinctly non-homogeneous character. Thus, while equations (1) and (2) may be applicable as a rough model for cement paste, they must be rewritten for concrete. In the remainder of this section, the conductivity equations are examined.

The three-dimensional generalization of equation (2) is the Laplace equation

$$\mathbf{J} = -\sigma_{phase} \nabla V \qquad (3)$$

Here σ_{phase} is the conductivity which is identical to the coefficient ckD in equation (2). The boundary conditions between the phases are given by the continuity of the voltage potential, V, and the continuity of the normal component of the flux vector.

Garboczi and Bentz [11,18] used equation (3) to derive analytical results for a "dilute limit" model for concrete. In this model, impermeable spheres (conductivity = 0, radius = r) with interfacial zones (conductivity = σ_{ITZ}, thickness = t) are placed in a uniform cement paste (conductivity = σ_{paste}). They showed that if the spheres are widely separated from each other, the one-dimensional form of equation (3) can be used with an average conductivity for the concrete. The result for the average concrete conductivity is

$$\sigma_{concrete} = \sigma_{paste} (1 + m [VF]) \qquad (4)$$

where the factor m depends only on the relative thickness and conductivity of the interfacial zone.

There are two limiting cases: no interfacial zone, in which m = - 3/2 and the aggregate reduces the conductivity, and a thin but highly conductive interfacial zone, in which m = 3 and the aggregate increases the conductivity. The corresponding results for the average concrete conductivity are

$$\sigma_{concrete} = \sigma_{paste} (1 - (3/2) [VF]) \qquad \text{(no ITZ)} \qquad (5)$$

$$\sigma_{concrete} = \sigma_{paste} (1 + 3 [VF]) \qquad \text{(highly conductive ITZ)} \qquad (6)$$

Garboczi and Bentz explained that there are higher-order terms that become important at even moderately small volume fractions. These higher-order effects are due to the interactions between closely spaced aggregates. While numerical techniques can be used to evaluate the higher-order terms, it is instructive to examine analytical results for some canonical problems. First, the interaction between two spherical aggregates is examined for the above two limiting cases for the interfacial zone.

Consider two spherical aggregates of radius r spaced at a distance s from each other. The centers of the aggregates are aligned in the direction of the applied electric field. The case of no interfacial zone is examined first. *Figure 2* shows the paths of the ion flux for far aggregate spacing (where equation (5) is accurate) and close spacing. The ion flux is diverted around the aggregate, resulting in increased tortuosity. For far aggregate spacing, the tortuosity effect is implicitly included in equation (5). However, it can be seen that for close spacing the tortuosity is decreased as compared with that for far spacing. Hence the tortuosity increases with increasing volume fraction of the aggregate.

Using an iterative method of images to solve Laplace's equation, the aggregate interaction effect is determined. The coefficient m in equation (4) becomes a function of the spacing between the aggregates

$$m = \frac{3}{2}\left(1 - \frac{1}{d^3} + \frac{1}{(1-d^2)^3} - \ldots\ldots\ldots\ldots\right) \qquad (7)$$

where $d = (2r + s)/r$ is the distance between the aggregate centers normalized by the radius r. For far aggregate spacing, where d becomes large, it can be seen that m approaches -3/2, which is the result in equation (5). However, as the aggregate spacing decreases, m also decreases. This is in agreement with *Figure 2* which shows a correspondingly smaller tortuosity effect. The coefficient m is plotted as a function of spacing s in *Figure 3*. It can be seen that the limiting value of m, where the aggregates are touching at $s = 0$, is $m = -1.35$.

Next, the case of a highly conductive interfacial zone is examined. *Figure 4* shows the paths of the ion flux for far aggregate spacing (where equation (6) is accurate) and close spacing. In this case, the ion flux is attracted to the conductive interfacial zone, which provides a rapid path for ion movement. *Figure 5* shows a surface plot of the voltages around the aggregate, and, according to equation (3), the ion flux is proportional to the steepness of the voltage surface. It can be seen that for close aggregate spacing, the ion flux between the aggregates becomes relatively large.

For a highly conductive interfacial zone, the coefficient m is

$$m = 3\left(1 + \frac{4-d^2}{2d^3} + \frac{2+3d^2-d^4}{2(-1+d^2)^3} + \ldots\ldots\ldots\ldots\right) \qquad (8)$$

which is plotted as a function of spacing s in *Figure 3*. For far aggregate spacing, in which d becomes large, it can be seen that m approaches 3, which is the result in equation (6). However, as the aggregate spacing decreases, m decreases, meaning that the concrete becomes less conductive.

This may be surprising in view of the high ion flux observed in *Figure 5*. The problem is that the ion flow must still pass through the cement paste before reaching the aggregate pair.

If a row of aggregate is considered, then the high ion flux seen in *Figure 5* will occur between each aggregate pair, resulting in percolation. To gain further insight into this percolation effect, Laplace's equation was examined for rows of spherical aggregate under a uniform electric field. To be compatible with equation (4), the volume fraction was kept constant, while the distance, d, between the centers of the spheres was varied. Using the method of images, it can be shown that the effect of percolation on the coefficient m is:

$$m = 3[1 + \frac{d^3}{(-1+d^2)^2} + \frac{(-1+d)^2}{(-2+d^2)^2} + \ldots\ldots\ldots\ldots\ldots\ldots] \quad (9)$$

Figure 6 shows a plot of m versus the spacing s between the spheres. As the spacing becomes small, m becomes large, indicating high conductivity. This is the expected percolation result. However, as the spacing becomes sufficiently large, m increases again. This is due to the fact that the volume fraction is kept constant: with larger spacing in the direction of the ion flow, there must be more rows of percolating spheres. (The very large values for m is due to the fact that the limit of highly conductive ITZ is considered.) Hence, for high volume fraction of aggregates percolation becomes a distinct possibility.

In summary, the analytical studies show that aggregate has a complex effect on the permeability. In the dilute limit, with far aggregate spacing, the aggregate effect is given by the relative thickness and conductivity of the ITZ. With close spacing, both the spacing between aggregate and percolation become prominent.

EXPERIMENTAL PROGRAM

Experimental Design Basis

An experimental study was conducted using the three phase model of the concrete permeability, aggregate, matrix and interfacial transition zone (ITZ), *Figure 7*, [4,11]. To simplify analysis, aggregates were considered impermeable; permeability contribution was limited to ITZ and cement matrix.

Materials

The materials used in the experiment have been illustrated in *Figure 8*. Alumina spherical balls were used as aggregate to provide impermeability to chloride ions. Also, spheres are easy to model and analyze. Two sizes of alumina balls, 6mm ϕ and 12mm ϕ were used to simulate grading. Ordinary Type 1 Portland cement was used as the binder.

Experimental Design

Two experimental variables, volume fraction of aggregate (VF) and proportion of large aggregate (AP) were considered.

$$\text{Volume Fraction of Aggregate (VF)} = \frac{\text{Volume of 6mm}\phi \text{ and 12mm } \phi \text{ Alumina Balls}}{\text{Total Volume of the Concrete Disk}}$$

$$\text{Proportion of Large Aggregate (AP)} = \frac{\text{Volume of 12mm}\phi \text{ Alumina Balls}}{\text{Volume of 6mm } \phi \text{ and 12mm } \phi \text{ Balls}}$$

Batches were designed with VF values of 0.25 and 0.5 and AP values of 0.16, 0.3, 0.7, and 0.84, *Figure 8*. But due to difference in specific gravity of cement and alumina , VF and AP values varied with location in each cylinder.

Experimental Procedure

Four batches of two cylinders each, 100 mm ϕ x 200 mm long, were cast using the above experimental design. The concrete was mixed using a high shear Omni mixer, Chiyoda OM-10E, and cured for about 90 days under water before being tested. Top and bottom 25 mm slices from each cylinder were discarded to eliminate segregation effects at the bottom. Remaining piece was sliced into 3-50 mm thick, top, middle and bottom, disks. Concrete disks were tested using the rapid chloride permeability test (RCPT), AASHTO - C1202-93, for 6 hours using 60 V. To prevent shrinkage cracking, slices were taken out of water only for testing. Exact measurements of VF and AP for each disk was made by baking in the oven and collecting the alumina balls. Some of the slices were processed using image analysis techniques. Each of these slices was sequentially sectioned at 3 mm maximum intervals and photographed, *Figure 9*. These were then scanned and used to reconstruct the three-dimensional slice using a computer program written for this purpose. A typical scanned slice photograph is shown in *Figure 10*.

EFFECT OF VARIABLES

The effect of volume fraction of aggregates and aggregate proportion on permeability is examined using tortuosity calculated as explained below and interfacial transition zone (ITZ). The amount of interfacial transition zone cannot be measured but is directly proportional to the surface area of aggregates, which can be easily measured.

Effect of Volume Fraction

The volume fraction has a significant effect on the permeability of the concrete specimens, *Figures 11*. We can draw the following conclusions from the graphs:

1. Generally, the permeability decreases with increasing volume fraction of alumina aggregates, for AP = 0.25 and AP = 0.85.
2. The effect of VF on permeability decreases with increasing VF. The effect becomes asymptotic for VF around 0.5

Discussion

Tortuosity is defined as the ratio of the average linear path of the chloride ions around the aggregates, L, and the thickness of the slice (or the shortest possible paths between points of consideration), L_0, *Figure 12* [3,9].

$$\text{Tortuosity, } T = \frac{< L >}{< Lo >} \tag{10}$$

Tortuosity was calculated by using the 3-D reconstructed 'computer' disk, as described earlier. Ions were assumed to go around each aggregate, always maintaining the initial linear path. Path length was measured at several hundred points starting from the top of the disk and going around each aggregate until bottom was reached. The tortuosity was the ratio of the average length of all these paths and thickness of each slice. As shown in the *Figure 13*, tortuosity was calculated as a function of permeability for VF = 0.5 and was found to decrease linearly with increasing permeability. The tortuosity was also found to be a linearly increasing function of VF for AP = 0.75, *(Figure 13)*. The data provided is limited, but all of the above conclusions are consistent with the modeling issues discussed earlier.

Tortuosity and interfacial transition zone (ITZ) both increase with increasing volume fraction of aggregates. Tortuosity decreases and interfacial zone increases permeability but tortuosity predominates, at least until VF of about 0.5. Similar effects have been found by other researchers [10,12,14,17, 21,22,23]. As discussed in the modeling issues, there is evidence to suggest that for higher VF's the interfacial zones start percolating, overriding any tortuosity effect. This leads to a net increase in permeability [23]. Similar effect was also found for concrete consisting of river gravel coarse aggregate of two average sizes, 6 mm ϕ and 12 mm ϕ, for w/c ratio of 0.3, *(Figure 14)*.

Effect of AP

The grading, simplified as the ratio of large aggregate (AP), also effects permeability, as shown in *Figure 15*. The following conclusions can be drawn:

1. For low volume fractions (VF = 0.25) , increasing proportion of large aggregate decreases permeability.

2. For higher volume fraction (VF = 0.5), permeability decreases for AP values up to 0.5. Thereafter, the permeability increases with increasing proportion of large aggregate.

Discussion

Tortuosity decreases with increasing proportion of large aggregates, *Figure 16,* for VF = 0.5. Surface area of aggregates, used as a surrogate for ITZ, decreases with increasing AP, *Figure 16.* Tortuosity decreases and interfacial zone increases permeability. For low AP values, large amount of surface area is available and ITZ effect overrides. Any increase of permeability due to decreasing tortuosity is overridden by decrease in ITZ. For higher AP (AP > 0.5) the decrease in tortuosity increases permeability; ITZ is more sporadically distributed and has less decreasing effect. Similar effects have been found by other researchers [22], although for water permeability.

PERMEABILITY OF CRACKED CONCRETE

Concrete production and curing methods in practice almost always create cracks in the matrix which may be due to several causes such as microcracking, shrinkage, loading, temperature, and delamination. Cracks in concrete create interconnected flow paths and hence cause greater permeability. This leads to deterioration of the structure which in turn leads to progressive cracking and finally failure of the structure. Hence study of the influence of cracking on permeability of concrete is of paramount importance. The present work relates cracking induced under loading to the water and chloride permeability of the concrete(25 mm thick) disks. Water permeability was measured using gravity as a pressure head [24]. Chloride permeability was measured by using RCPT (ASTM C1202-93).

Feedback Controlled Splitting Cracks

Concrete is a quasi-brittle material that allows a slow stable crack growth before the material breaks apart completely, showing strain softening when the applied loading is beyond its peak value. Based on this material behavior, a stable crack growth in concrete can be obtained by monitoring and controlling some physical quantities which are associated with deformation of the specimen. In the other word, cracks may be generated in a concrete specimen without breaking the specimen completely apart when an appropriate displacement-controlled testing system is used. For the whole description of the feedback controlled splitting test refer to [25].

During the feedback controlled splitting test, a cylindrical specimen (100 mm ϕ x 25 mm thick) is loaded diametrically under Brazilian test configuration, *Figure 17.* A single LVDT is mounted on each side of the specimen, perpendicular to the loading direction, so as to monitor the crack opening displacement (COD) on both sides. The LVDTs each have a range of $\pm$0.5 mm. Plywood strips, 25 mm wide and 3 mm in thickness, are placed between the loading plates and the specimen to prevent crushing at the loading points.

The 4.4 MN test machine is used with a 490 kN strain gage load cell to measure the force (a calibrated range of 49 kN was used for the 25 mm thick specimens). The average displacement of the two LVDTs is digitally calculated and used as the feedback control. The control parameter, the average crack opening displacement, is increased at a constant rate of 0.2 μm/sec. The specimens are loaded to a design crack width under the feedback control and then, unloaded under load control. The time, force, stroke, and crack opening displacement from each LVDT as well as their average (used as the feedback signal) is all recorded during the testing. The loading patterns for different crack widths and maximum load are described in [25]. Some common variables effecting cracking and permeability are described below.

EFFECTS OF VARIABLES ON CRACKING

Effect of Material Composition on Cracking

Variation of cracking characteristics with materials was explored using paste, normal strength concrete (NSC) and high strength concrete (HSC). The materials used for paste consisted of Type 1, Portland cement and water/cement ratio of 0.41. NSC, in addition to above, contained river gravel (maximum aggregate size of 9.5 mm, sp. gravity of 2.4), and graded river sand. HSC composition was similar to NSC except for silica fume, super plasticizer and water/cement ratio of 0.29. 25 mm thick and 50 mm thick disks of each material were cracked using the feedback controlled test described above. For each of the cracked disks, actual crack mouth opening displacement (CMOD) before and after loading was recorded and plotted, *Figure 18*. Crack control of paste disks was difficult; several trials were needed before disks with stable crack formation could be obtained. Brittle nature and absence of any bridging mechanisms contributed to the above behavior. NSC and HSC slices exhibited stable crack formation. Crack recovery is defined as the difference between crack width under load and after unloading. The advantage of the feedback control test is that the final crack widths are accurately known. The following conclusions can be noted from *Figure 18*:

1. Crack recovery for all the materials lies pretty much within a narrow band except for NSC, 25 mm and 50 mm thick, disks. One possible reason is that cracks in NSC go around aggregates (through weak interfaces) leading to crack tortuosity and wider fracture process zones and hence less crack recovery. Cracks in HSC and paste are not deflected by aggregates and consequently, have a narrow fracture process zone leading to greater recovery.
2. Thickness does not effect the crack recovery behavior of the material.

Effect of Crack Roughness on Flow

In order to quantify the effects of the cracks, following formula based on the flow through a parallel sided slot has traditionally been used to describe a relationship between measured and the calculated laminar water flow rate[26,27]:

$$q = C\Delta h \tag{11}$$

where,

C = conductance, which depends on geometry of the flow cross-section and fluid properties, cm^2/s

Δh = head loss between the two points being considered

$$C = \varepsilon \frac{g w^3 l}{12 \nu d} \tag{12}$$

where,

g = gravitational attraction, cm^2/s

w = average crack width, cm

d = thickness of the disk, cm

ν = kinematic viscosity of the fluid, cm^2/s

ε = crack roughness coefficient

l = length of the crack, cm

Cracks were assumed to go through the specimen end to end. The length of crack for parallel sided slot was based on actual length of the crack. The crack width of the cracks was assumed to be equal to the average crack width measured by LVDT's. The following conclusions can be drawn from *Figure 19*:

1. The crack roughness coefficient (difference between ideal and actual flow), ε, increases up to about 100 microns. For cracks with widths 180 microns and larger the coefficient comes very close to the actual value; gap narrows for larger cracks. Hence the idealization of flow through parallel sided slot works better for large crack widths.
2. The length of crack increases with increasing crack widths [25, Fig. 6] lowering the effect of uncracked matrix. For large crack widths, most of the matrix is cracked and assumption of the parallel sided slot is valid. For smaller crack widths, cracked area is small, and large amount of flow is through the matrix which is fairly uncracked (and hence slow) and, hence, the above assumption is not valid.

Effect of Water and Rapid Chloride Permeability Tests

NSC disks, 25 mm thick (100 mm ϕ) , were tested for water permeability using a falling head permeater [24] and for chloride permeability using RCPT (ASTM C1202-93) using different crack widths, *Figure 20-21*. Chloride permeability of HSC Slices, 25 mm thick (100 mm ϕ), were determined using RCPT test, *Figure 22*. The following conclusions can be drawn:

1. Both water and chloride permeabilities increase with increasing crack widths for NSC concrete, *Figure 20* . Similar trend in chloride permeability is observed for HSC disks, *Figure 22*. Increasing crack width thus leads to greater chloride and water permeabilities which ultimately lead to progressive cracking and failure of the structure.

2. Water permeability is more sensitive to crack width for NSC samples than RCPT test, *Figure 20*. In other words, the water preferentially flows through cracks unlike chloride ions which also flow through the uncracked matrix.
3. Water and chloride permeability for NSC disks are linearly related for wider crack widths (> 60 microns). Relationship is not clear for smaller crack widths (< 45 microns), *Figure 21*. Linear relations for uncracked concrete have been observed [28].
4. The rapid chloride permeability test was less sensitive for crack widths for NSC than HSC, *Figures 20 and 22*. Permeable matrix diffuses the flow of ions for NSC, whereas for dense matriced HSC slices the ions are concentrated towards the cracks. The perviousness of the surrounding matrix effects the RCPT results.

CONCLUSIONS

A new approach integrating statistics with concrete technology is described for studying and modeling the microstructure and mesostructure of concrete. Complete durability approach for concrete structures requires permeability, cracking characteristics, and strength of the material. Permeability of concrete is effected by the volume fraction of aggregates, tortuosity of ion path, and interfacial transition zone (ITZ) around each aggregate. The volume fraction of aggregates decreases the permeability of concrete by increasing tortuosity. Increased amount of aggregates can lead to percolation and hence increased permeability. Modeling concrete as a two phase material consisting of spherical aggregates and homogeneous matrix phase can explain the aforementioned effects. Increasing proportion of large aggregates decreases permeability but higher volume fractions can reverse the trend. A simple definition of tortuosity and interfacial transition zone can be used to explain the above results. Cracks effect the viability of a structure by facilitating the entry of deleterious substances in concrete. Stable crack formation in concrete can be achieved by feedback controlled splitting. Crack recovery in a material is a function of strength of its ITZ which govern the tortuosity of the crack path. Cracks in concrete can be modeled using laminar flow through a parallel side slot for crack widths about 180 microns or larger. Water permeability is a better indicator of crack width than RCPT. Impenetrability of the surrounding matrix governs the effectiveness of RCPT in detecting cracks.

ACKNOWLEDGMENTS

This research is supported by NSF grant DMS9313013 to National Institute of Statistical Sciences. Support from the NSF Center for Science and Technology of Advanced Cement Based Materials is also appreciated.

REFERENCES

1. Shah, S. P. and Wang, K."Microstructure, Microcracking, Permeability, and Mix Design Criteria of Concrete," Submitted for Publication, 1997.
2. Karr, A. F. "Research Plan: Microstructure-Permeability Relationships for Concrete," July 27, 1994.
3. Sahimi, M "Flow and Transport in Porous Media and Fractured Rock," VCH, 1995, pp. 1-10 and 51-53.
4. Bentz, D. P., Garboczi, E. J., and Landgren, E.S. "Multiscale Microstructural Modeling of Concrete Diffusivity: Identification of Significant Variables," ASTM Cement, Concrete and Aggregate, in press.
5. De La Rue, R.E. and Tobias, C.W. "On the Conductivity of Dispersions," Journal of Electrochemical Society, v.106, no. 9, 1959.
6. Hall, Christopher, "Barrier Performance of Concrete: A review of fluid transport theory," Materials and Structures, 1994, 27, 291-306, RILEM TC-146: Tightness of Concrete with respect to fluids.
7. Dogu, T. and Dogu, G. "A Grain Model for Catalyst Tortuosity," Chemical Engineering Communications, v. 103, pp 1-9, 1991.
8. Sharma, R. K. and Cresswell, D.L. "Effective Diffusion Coefficients and Tortuosity Factors for Commercial Catalysts," Industrial and Engineering Chemical Research, v.30, July 1994, pp. 1428-33.
9. Suman, R. and Ruth, D. "Formation factor and Tortuosity of Homogeneous Porous Media," Transport in Porous Media 12:185-206, 1993.
10. Delagrave, A., Bigas, J.P., Ollivier, J.P., Marchand, J. and Pigeon, M. "Influence of the Interfacial Zone on the Chloride Diffusivity of Mortars," Cement and Concrete Research, 1994.
11. Garboczi, E. J. and Bentz, D.P. " Analytical Formulas for Interfacial Transition Zone Properties," MRS, Fall 1996, preprint.
12. Garboczi, E.J., Schwartz, L.M., and Bentz, D.P." Modeling the Influence of the Interfacial Zone on the DC Electrical Conductivity of Mortar," ACBM Journal, Elsevier Science, 1995.
13. Johansen, V. and Anderson, P.J. "Particle Packing and Concrete Properties," Material Science of Concrete II, pp. 111-147.
14. Ollivier, J.P. and Massat, M. "The effect of the transition zone on transfer properties of concrete," Interface Transition Zone in Concrete, Edited by J.C. Maso, RILEM Report 11.
15. Schwartz, L.M., Martys, N., Bentz, D.P., Garboczi, E. J. and Torquato, S."Cross-property relations and permeability estimation in model porous media," Physical Review E, v. 48, no.6, December 1993.
16. Saito, M. and Kawamura, M. "Effects of Cement Paste-Aggregate Interfacial Zone on the Chloride Permeability of Concretes with a low:cement ratio," Proc. International Brittle Matrix Composites 4, Edited by Brandtl, A. M., Li, V. C. and Marshall, I. H., pp. 484-491, Warsaw, September 1994.
17. Tumidajski, P. T. "Electrical Conductivity of Portland Cement Mortars," Cement and Concrete Research, v. 26, no. 4, pp. 529-534, 1996.

18. Garboczi, E. J. and Bentz, D. P. "The effect of Interfacial Transition Zone on Concrete Properties: The Dilute Limit," 4th ASCE Materials Conference, Wash. D.C., 11/96.
19. Gjϕrv, O. E. and Zhang, T. "An Electrochemical Method for Accelerated Testing of Chloride Diffusivity in Concrete," Cement and Concrete Research, Vol. 24, 8, pp. 1534-1548, 1994.
20. Zhang, T. and Gjϕrv, O. E. "Effect of Ionic Interaction in Migration Testing of Chloride Diffusivity in Concrete," Cement and Concrete Research, paper submitted.
21. Philipse, A. P. and Pathmamanoharan, C. " Liquid Permeation (and Sedimentation) of Dense Colloidal Hard Sphere Packings," Journal of Colloidal and Interface Science, 159, 96-107, 1993.
22. Thies-Weesie, and Philipse, A.P. "Liquid Permeation of Bidisperse Colloidal Hard Sphere Packing and Kozeny Carman Scaling Relation," Journal of Colloidal and Interface Science, 162, pp. 470-480, 1994.
23. Houst, Y.F. "Influence of Aggregate Concentration on the Diffusion of CO2 and O2," Interfaces in Cementatious Composites, Edited by J.C. Maso, RILEM
24. Ludirdja, D. L., Berger, R.L., and Young, J.F. "Simple Method of Measuring Water Permeability of Concrete'" ACI Materials Journal, n0. 86-M38, 5, September, 1989.
25. Wang, K., Jansen, D.C., and Shah, S.P. " Permeability Study of Cracked Concrete," Cement and Concrete Research, Vol.27, N0.3, pp. 381-393, 1997.
26. Tsukamato, M. "Tightness of Fiber Concrete," Darmstadt Concrete, 1992.
27. Tsukamato, M. and Worner, J.D. "Permeability of Cracked Fiber-Reinforced Concrete," Darmstadt Concrete, 1992.
28. Whiting, D. "Permeability of Selected Concretes," Permeability of Concrete, Whiting, D. and Walitt, A., ed., ACI SP-108, pp. 195-222.

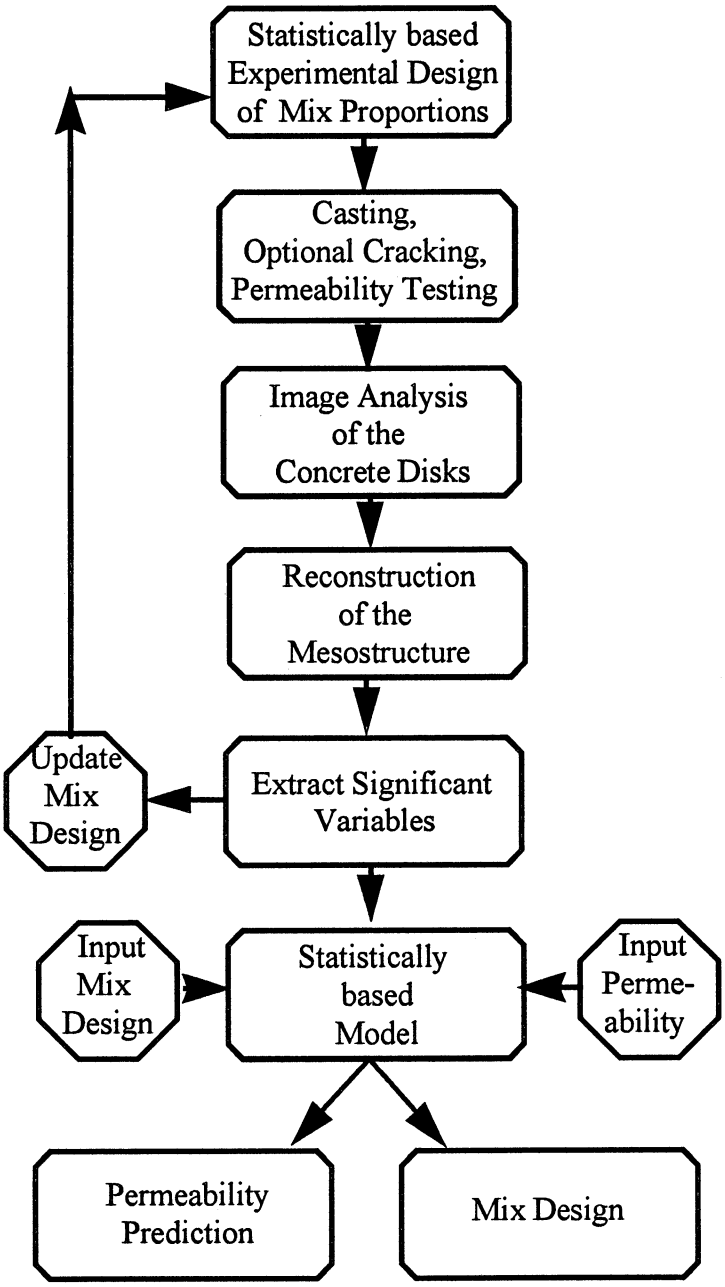

Figure 1. Objectives and Research Plan

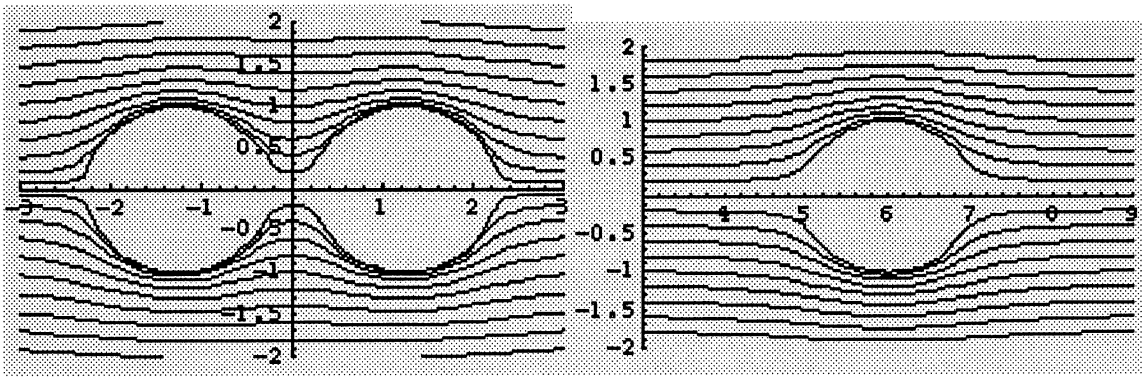

(a) Spacing = 0.5 radians (b) Spacing = 10 radians

Figure 2. Ion flux around spherical aggregate with no interfacial zone

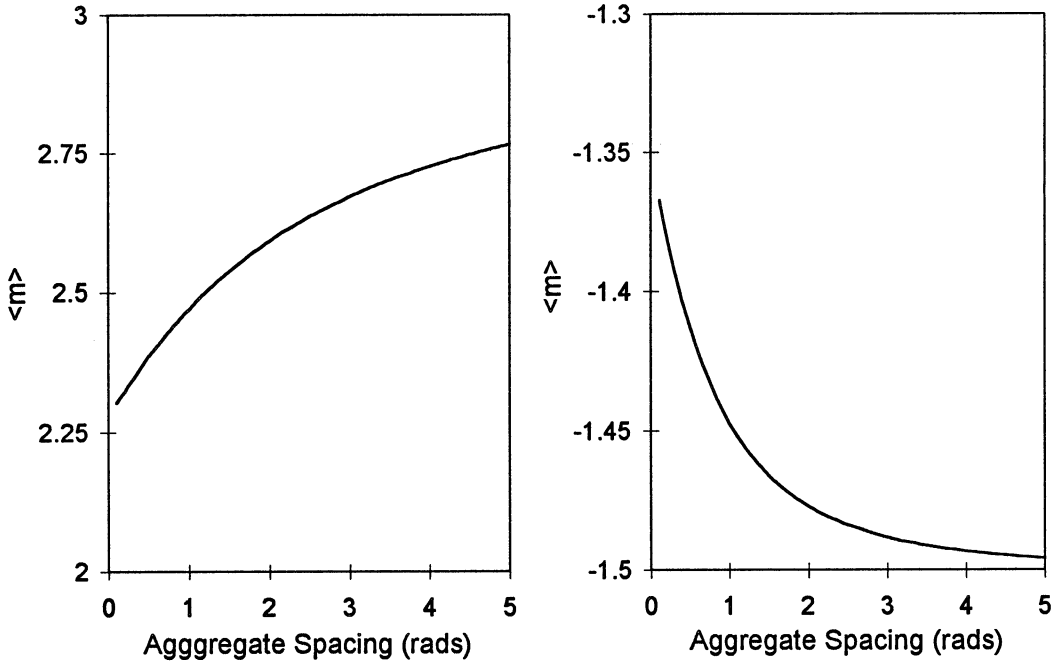

(a) Highly conductive Interfacial Transition Zone (b) No Interfacial Zone

Figure 3. Coefficient <m> as a function of the aggregate spacing

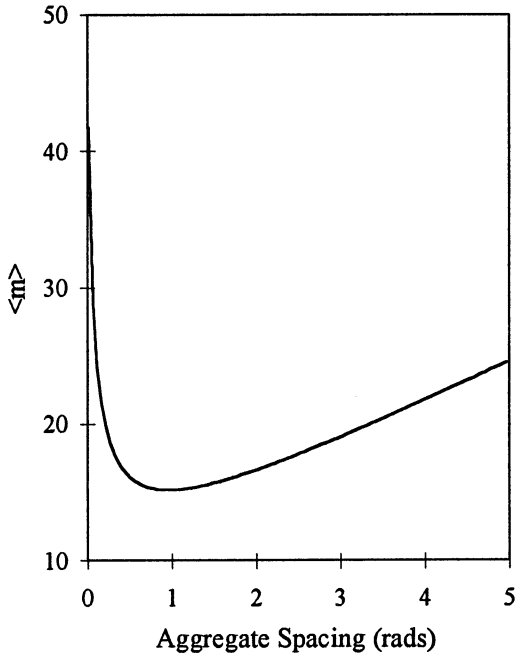

Figure 6.Effect of Percolating Spheres on Conductivity

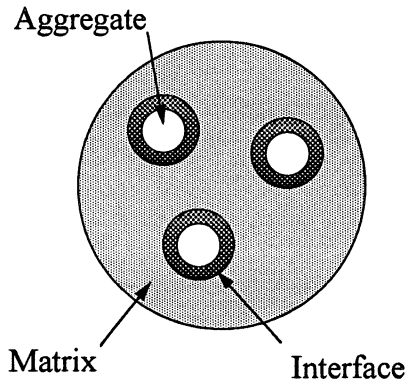

Figure 7. Three Phase Concrete Model

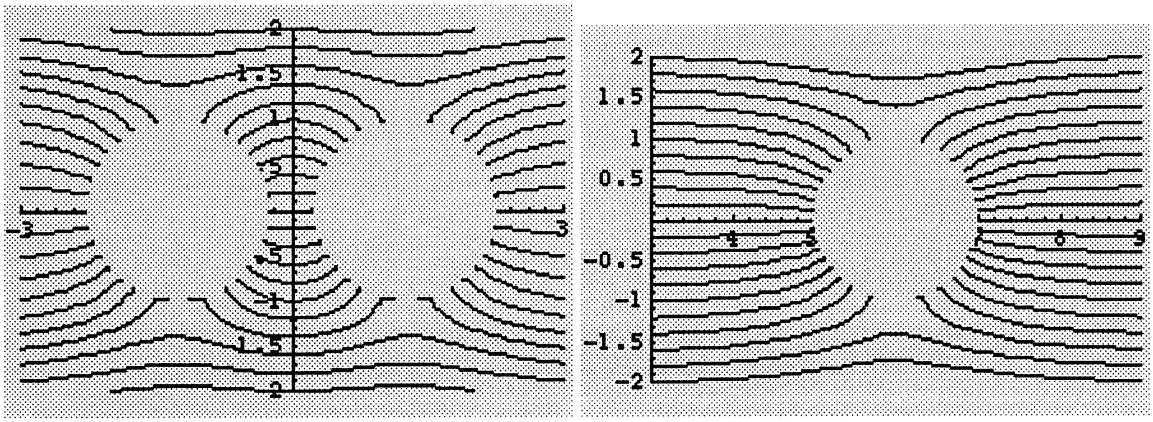

(a) Spacing = 0.5 radians **(b) Spacing = 10 radians**

Figure 4. Ion flux around spherical aggregate with highly conductive interfacial zone

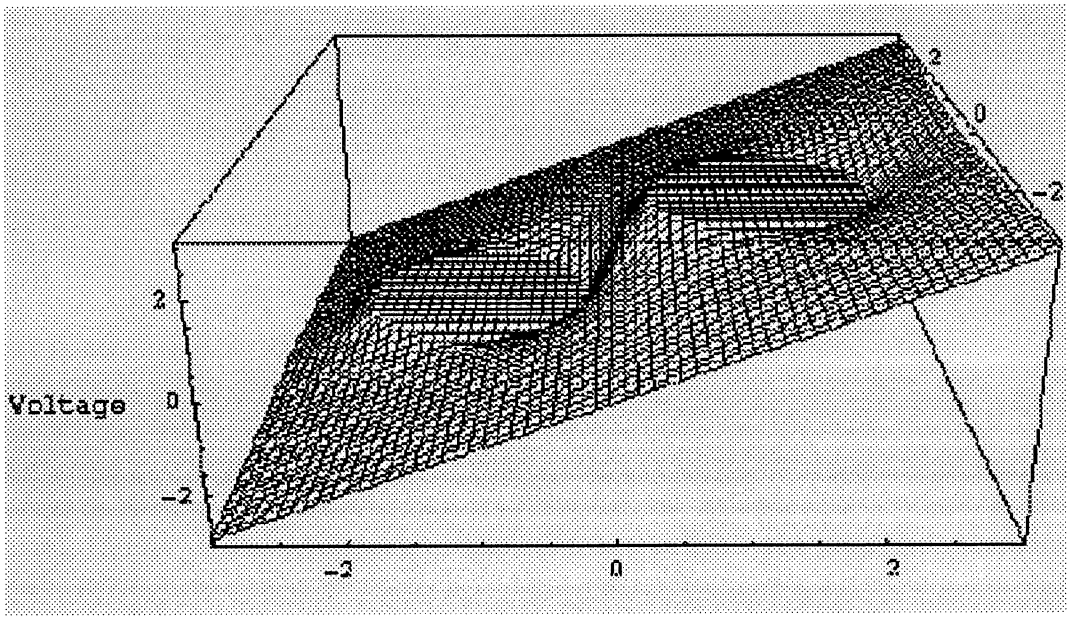

Figure 5. Voltages around aggregate with highly conductive interfacial transition zone

Materials and Processing	
Cement	Type 1
Aggregate	Alumina Spheres, 6mm ϕ and 12 mm ϕ , Specific Gravity = 3.4
Water/Cement Ratio	0.3
High Shear Mixer	Chiyoda OM-10E
Curing	28 days under water
Volume Fraction (VF)	0.25, 0.5
Proportion of Large Aggregate (AP)	0.16, 0.3, 0.7, 0.84

Figure 8. Experimental Description

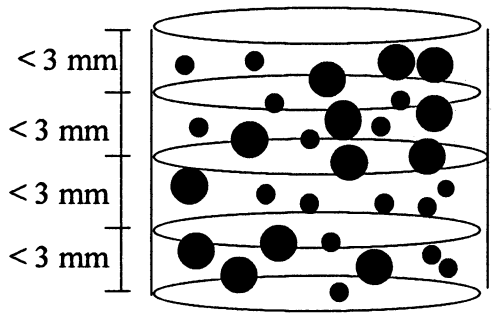

100 mm ϕ x 50 mm thick

Figure 9: Slicing Disks for Image Analysis

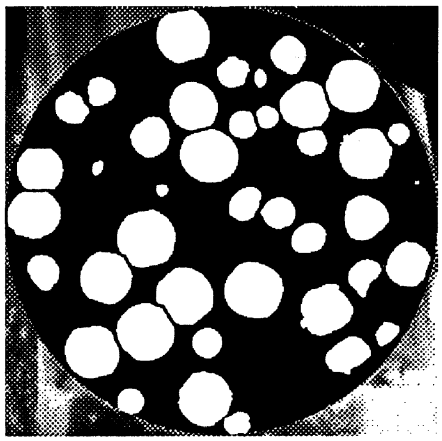

Figure 10. Actual Slice

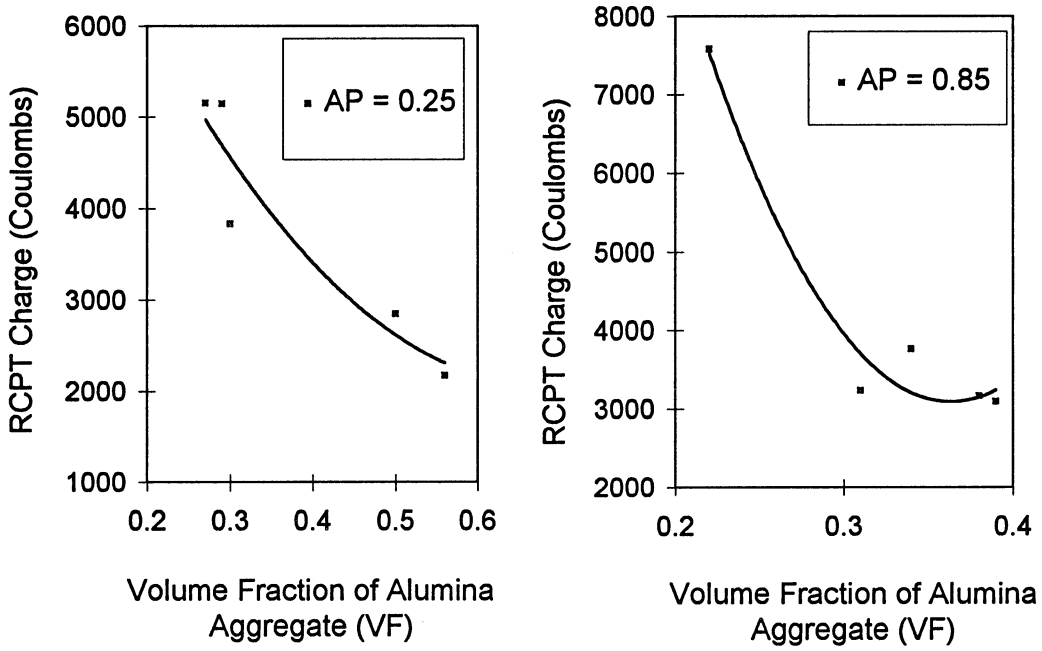

Figure 11. Variation of Volume Fraction of Alumina Aggregates (VF) and RCPT Charge

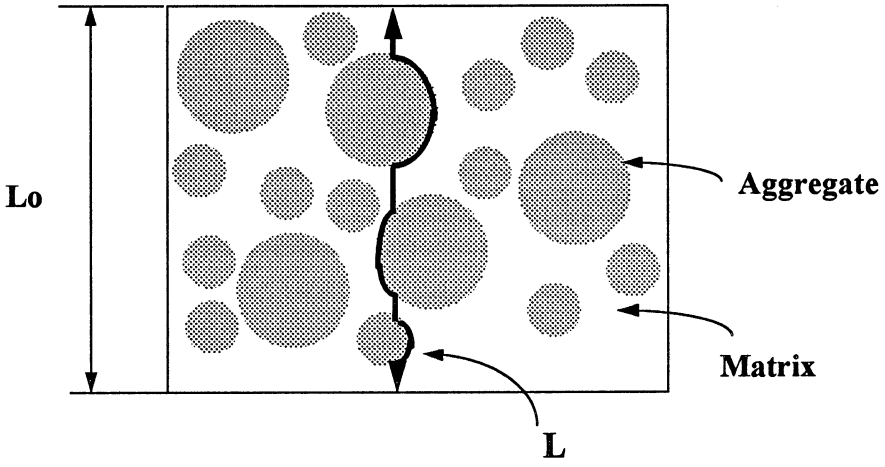

Tortuosity = L/Lo

Figure 12. Definition of Tortuosity for Concrete Slice

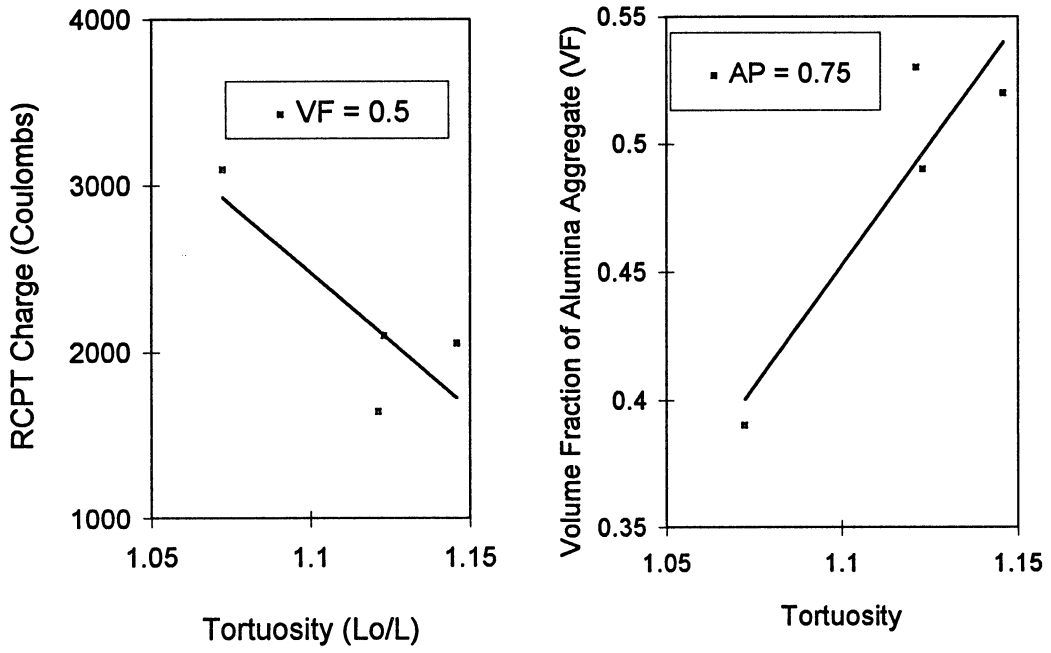

Figure 13. Variation of Tortuosity with RCPT Charge and Volume Fraction of Alumina Aggregates

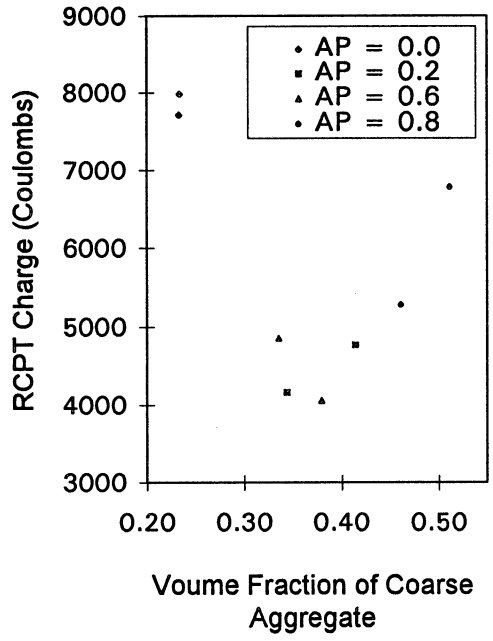

Figure 14. Variation of Gap-graded River Gravel with RCPT Charge (Coulombs)

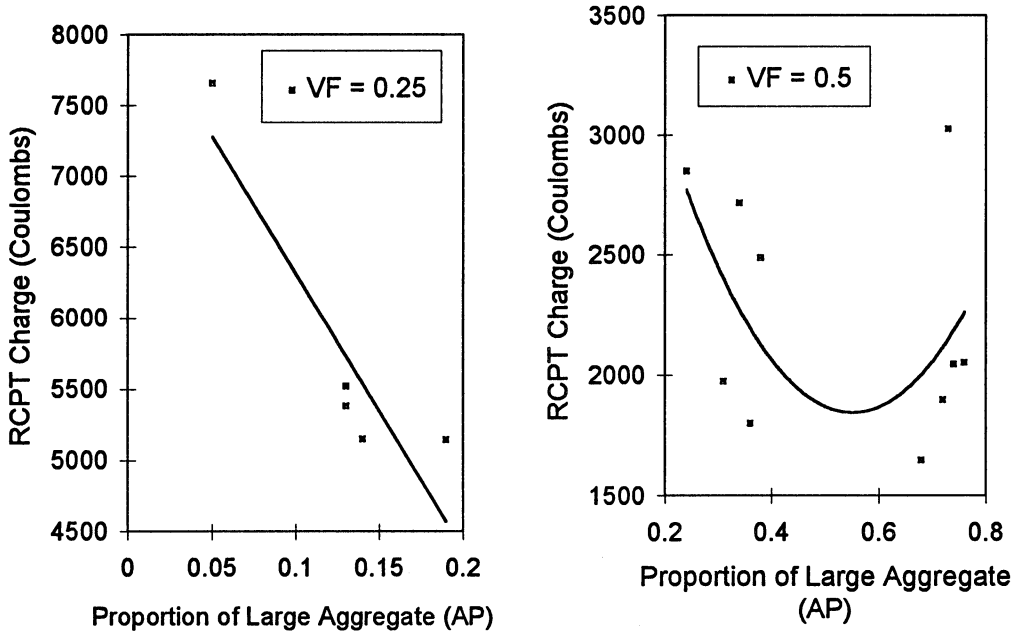

Figure 15. Variation of Proportion of Large Aggregate (AP) with RCPT Charge

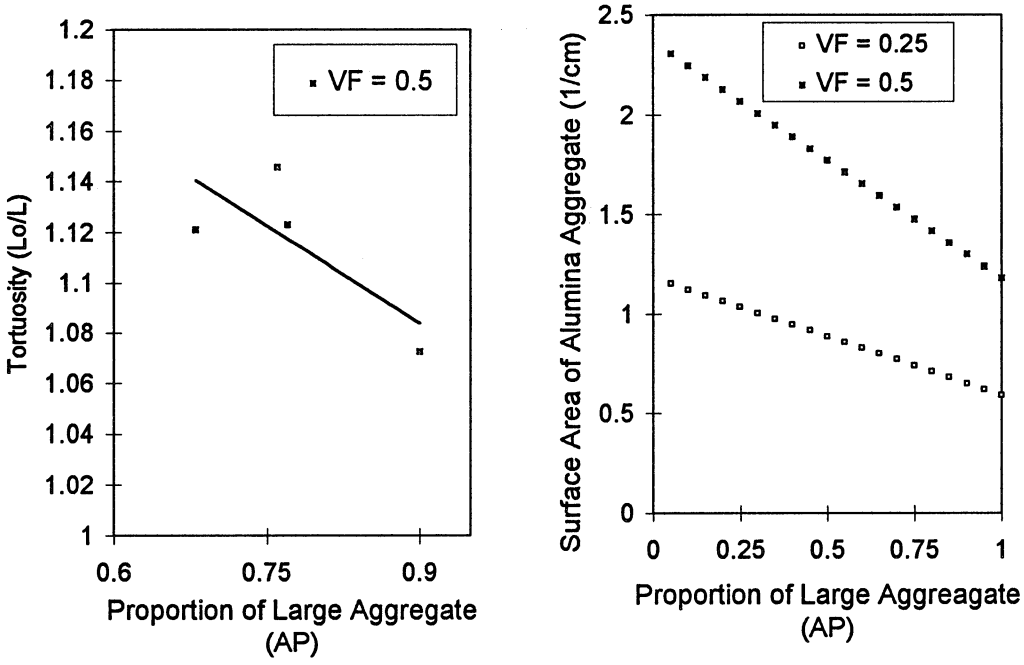

Figure 16. Variation of Proportion of Large Aggregate with Tortuosity and Surface Area of Alumina Aggregate

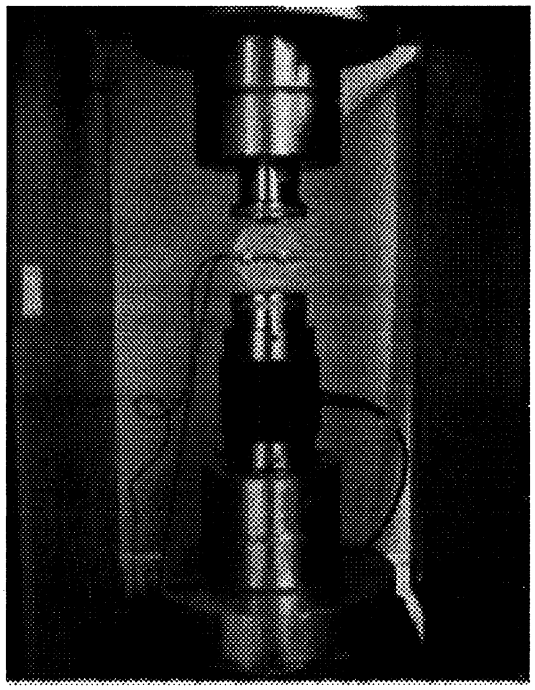

Figure 17. Feedback Controlled Splitting Tensile Test

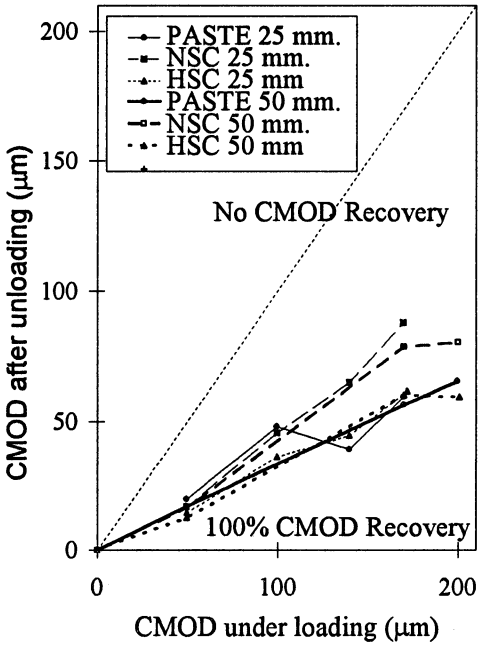

Figure18. Effect of Different Materials on Crack Recovery

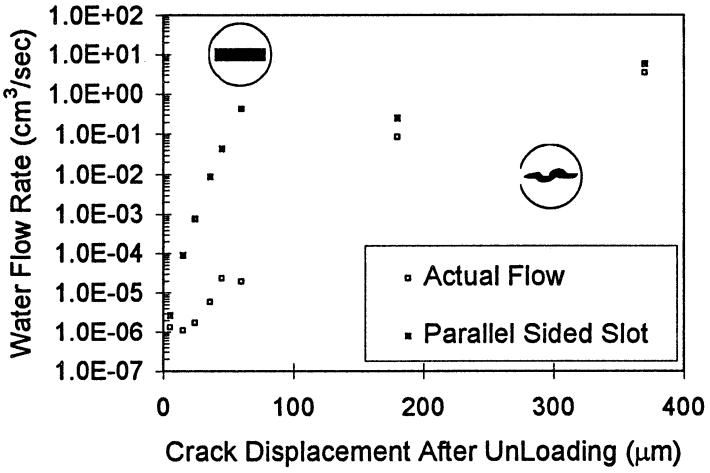

Figure 19. Effect of Crack Roughness (Tortuosity) on Flow Rate

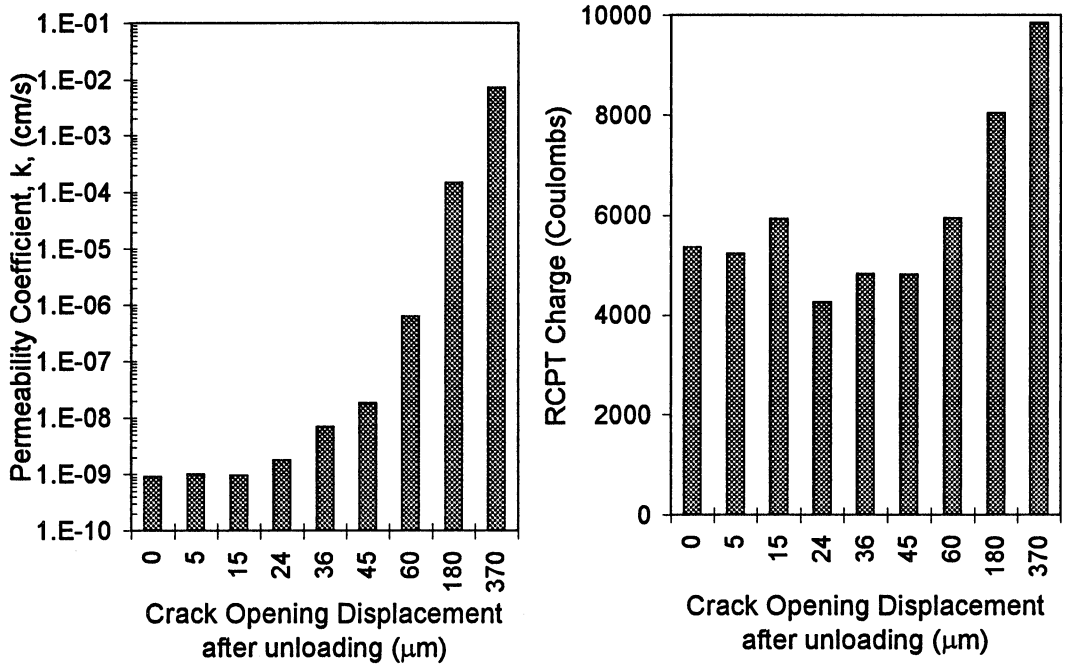

Figure 20. Water and RCPT Permeabilities for 25 mm thick, NSC Disks

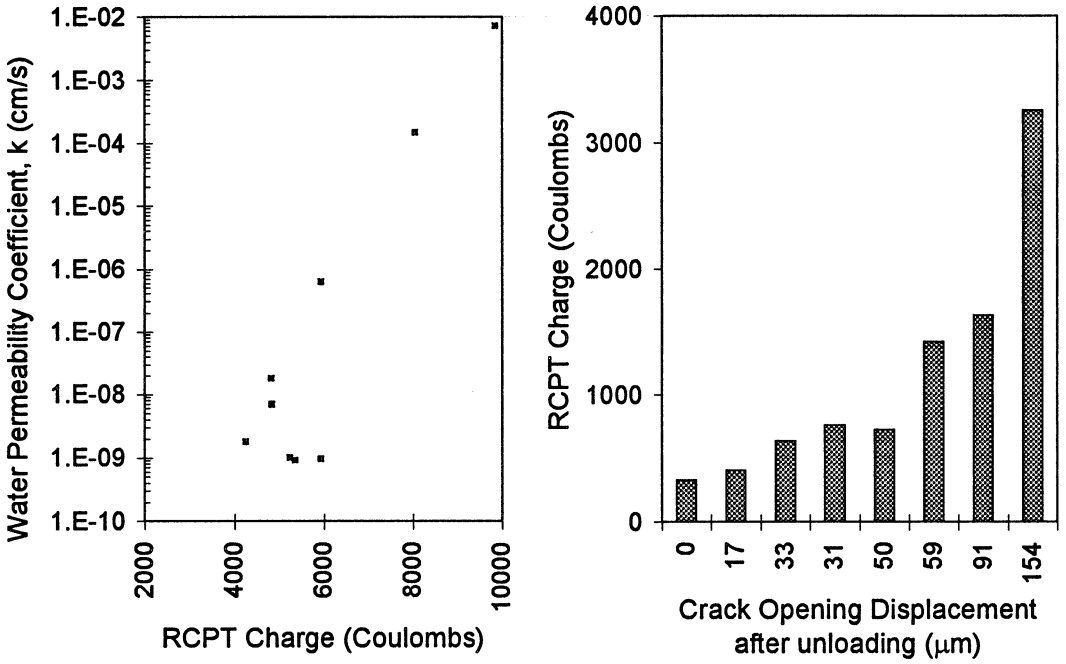

Figure 21. Comparison of Water and RCPT Permeabilities for NSC Disks

Figure 22. RCPT Permeability for 25 mm HSC Disks